Coulomb energy and gluon distribution in the presence of static sources

Adam P. Szczepaniak and Pawel Krupinski

Physics Department and Nuclear Theory Center, Indiana University, Bloomington, Indiana 47405, USA

(Received 19 November 2005; published 21 February 2006)

We compute the energy of the ground state and a low-lying excitation of the gluonic field in the presence of static quark-anti-quark ($q\bar{q}$) sources. We show that for separation between the sources less then a few fm the gluonic ground state of the static $q\bar{q}$ system can be well described in terms of a mean field wave functional with the excited states corresponding to a single quasiparticle excitation of the gluon field. We also discuss the role of many particle excitations relevant for large separation between sources.

DOI: 10.1103/PhysRevD.73.034022 PACS numbers: 12.38.Aw, 11.10.Ef, 12.38.Cy, 12.38.Lg

I. INTRODUCTION

Recent lattice simulations lead to many new theoretical insights into the dynamics of low-energy gluon modes [1–6]. In the quenched approximation aspects of confinement emerge from studies of the gluonic spectrum produced by static color sources. In the following we will focus on the pure gluon dynamics (the role of dynamical quarks in the screening of confining gluonic strings has recently been studied in [7]).

Lattice studies indicate that with relative separations between two color sources, $R \gtrsim 1.7$ fm, the ground state energy obeys Casimir scaling [8,9]. This means that the spectrum of gluon modes generated by static color sources depends on the dimension of the color representation of the sources rather than on the N-ality of the representation (which is related to the transformation property of a representation with respect to the group center) [10]. For example, for two sources in the fundamental representation, lattice computations show, as expected, that energy grows linearly with the separation between the sources. However, also for sources in the adjoint representation (with N-ality of zero), lattice produces a linearly rising potential, even though for vanishing N-ality screening is expected to saturate the potential. Screening comes from the production of gluon pairs and vanishes in the limit of a large number of colors. Casimir scaling is thus telling us that there is, at least in the energy range relevant for hadronic phenomenology, a simple, universal (source independent) description of the confining string.

The lattice spectrum of gluonic modes generated by sources in the fundamental representation, i.e., a static quark-antiquark ($q\bar{q}$) pair, has been extensively studied in [1,2]. The ground state energy which as a function of the $q\bar{q}$ separation is well represented by the Cornell, ''Coulomb + linear'' potential and the spectrum of excited gluonic modes have been computed. The excited gluonic modes lead to excited adiabatic potentials between the sources in the sense of the Born-Oppenheimer approximation with the quark sources and gluonic field corresponding to the slow and fast degrees of freedom, respectively [11,12]. The gluonic wave functional of these modes can be classified analogously to that of a diatomic molecule. The good quantum numbers are $\Lambda = 0(\Sigma), 1(\Pi), 2(\Delta), \ldots$ which give the total gluon spin projection along the $q\bar{q}$ axis, $PC = +1(g), -1(u)$ which correspond to the product of gluon parity and charge conjugation, and $Y = \pm 1$ which describes parity under reflection in a plane containing the $q\bar{q}$ axis. The ground state corresponds to $\Lambda^Y_{PC} = \Sigma^+_g$. The lattice calculations show that the first excited state has the Π_u symmetry (for $\Lambda \neq 0$, $Y = \pm 1$ states are degenerate) and thus has $PC = -1$.

The lattice spectrum of gluonic excitations is well reproduced by the bag model [13,14]. The crucial feature of the model that makes this possible is the boundary condition, which requires the longitudinal component of the chromoelectric and transverse components of the chromomagnetic field of the free gluon inside the cavity to vanish at the boundary of the bag. This results in the transverse electric (TE) mode with pseudovector, $J^{P,C} = 1^{+,-}$, quantum numbers having the lowest energy, which leads to the Π_u adiabatic potential being the lightest from among the excited gluonic states in the $q\bar{q}$ system. In another model, the nonrelativistic flux tube model [15], the $PC = +1$ quantum numbers of the low-lying gluon mode result from associating a negative parity and a positive charge conjugation to the lowest order transverse phonon (unlike that of a vector field). This also results in the Π_u quantum numbers for the first excited adiabatic potential. Finally in a QCD based quasiparticle picture the intrinsic quantum numbers of the quasigluons are $J^{P,C} = 1^{-,-}$, that of a transverse vector field [16,17]. If the first excited adiabatic potential between $q\bar{q}$ sources is associated with a single quasigluon excitation and this quasigluon interacts via normal two-body forces with the sources, then, one expects the quasigluon ground state wave function to be in an orbital S wave, which, in turn, leads to the net $PC = +1$ and the Π_g symmetry for this state. This is in contradiction with the lattice data as noted in [17]. The bag model and the flux tube model give the right ordering of the spectrum of low-lying gluonic excitations, even though they are based on very different microscopic representations of the gluonic degrees of freedom.

There are indications from lattice simulations of various gauge models that the adiabatic potentials approach that of

the flux tube, or better stringlike spectrum for $q\bar{q}$ separations larger than $R \gtrsim 3$ fm [18], however, the situation for QCD is far less clear [2]. In particular, for large separations between the sources the splitting between nearby string excitations is expected to fall off as $\propto \pi/R$. The lattice results indicate, however, that the spacing between the adiabatic potentials is close to constant. At distances $R \lesssim 0.2$ fm the flux tube model becomes inadequate while QCD is expected to become applicable. For example as $R \to 0$, the Coulomb potential between the quark and the antiquark in the color octet is repulsive, and, indeed, the results of lattice calculations do seem to have that trend. The bag model attempts to combine the perturbative and long-range, collective dynamics by using noninteracting fields inside a spherically symmetric bag and deforming the bag to a stringlike shape as the separation between the sources increases. A self-consistent treatment of bag and gluon degrees of freedom is, however, lacking.

Another model which aims at relating the stringlike excitations at large $q\bar{q}$ separations with the QCD gluon degrees of freedom is the gluon chain model [6,19] and versions thereof [20]. The model is based on the assumption that as the separation between the sources increases pairs of constituent gluons are created to screen the charges in such a way that the Fock space is dominated by a state with a number of constituent gluons, which grows with the $q\bar{q}$ separation. Recently, support for the gluon chain model came from lattice studies of the Coulomb energy of the $q\bar{q}$ pair [21,22]. As shown in [23], at fixed R, Coulomb energy bounds the true exact (from Wilson line) energy from above. The Coulomb energy is defined as the expectation value of the Coulomb potential in a state obtained by adding the $q\bar{q}$ pair to the exact ground state of the vacuum, i.e., without taking into account vacuum polarization by the sources. The addition of sources changes the vacuum wave functional by creating constituent gluons as described by the gluon chain model.

In this paper we discuss the structure of the $q\bar{q}$ state in terms of physical, transverse gluon degrees of freedom. In particular, we focus on the importance of constituent gluons in describing the excited adiabatic potentials. For simplicity and to make our arguments clearer, we concentrate on excited adiabatic potentials of single, $\Lambda_{PC}^{Y} = \Sigma_g^+$, symmetry. A description of the complete spectrum of excited potentials will be presented in a following paper. Our main finding here is that a description based on a single (few) constituent gluon excitation is valid up to $R \sim$ few fm, with the gluon chain turning in, most likely, at asymptotically large $q\bar{q}$ separations. Consequently, we show how the gluon chain model can emerge in the basis of transverse gluon Fock space.

In Sec. II we review the Coulomb gauge formulation of QCD and introduce the Fock space of quasigluons. In Sec. III we review the computation of the ground state and the excited Σ_g^+ potentials. There we also discuss the role of multiparticle Fock sectors and a schematic model of the gluon chain. A summary and outlook are given in Sec. IV.

II. COULOMB GAUGE QCD

In the Coulomb gauge gluons have only physical degrees of freedom. For all color components $a = 1, \ldots, N_C^2 - 1$ the gauge condition, $\boldsymbol{\nabla} \cdot \mathbf{A}^a(\mathbf{x}) = 0$, eliminates the longitudinal degrees of freedom and the scalar potential, $A^{0,a}$, becomes dependent on the transverse components through Gauss's law [24]. The canonical momenta, $\Pi^a(\mathbf{x})$, satisfy $[\Pi_i^a(\mathbf{x}), A_j^b(\mathbf{y})] = -i\delta_{ab}\delta_T^{ij}(\boldsymbol{\nabla})\delta^3(\mathbf{x}-\mathbf{y})$ where $\delta_T^{ij}(\boldsymbol{\nabla}) = \delta^{ij} - \nabla^i\nabla^j/\boldsymbol{\nabla}^2$; in the Schrödinger representation, the momenta are given by $\Pi^a(\mathbf{x}) = -i\delta/\delta\mathbf{A}^a(\mathbf{x})$. More discussion of the topological properties of the fundamental domain of the gauge variables can be found in [25]. The full Yang-Mills (YM) Hamiltonian with gluons coupled to static $q\bar{q}$ sources in the fundamental representation is given by

$$H = H_0 + H_{Qg} + H_{QQ}, \tag{1}$$

where H_0 is the YM Hamiltonian containing the kinetic term and interactions between transverse gluons. The explicit form of the YM Hamiltonian, H_0, can be found in [24]. The coupling between $q\bar{q}$ sources and the transverse gluons, H_{Qg}, is explicitly given by

$$H_{Qg} = \int d\mathbf{x}d\mathbf{y}\rho_Q^a(\mathbf{x})K[\mathbf{A}](\mathbf{x}, a; \mathbf{y}, b)\rho^b(\mathbf{y}), \tag{2}$$

where $\rho_Q = h^\dagger(\mathbf{x})T^a h(\mathbf{x}) - \eta^\dagger(\mathbf{x})T^{*a}\eta(\mathbf{x})$ is the color density of the sources with h and η representing the static quark and antiquark annihilation operators, respectively; $\rho = -f_{abc}\mathcal{J}^{-1}\Pi^b(\mathbf{x})\mathcal{J}\cdot\mathbf{A}^c(\mathbf{x})$ is the gluon charge density operator and K is the non-Abelian Coulomb kernel,

$$K[\mathbf{A}](\mathbf{x}, a; \mathbf{y}, b) = \frac{g^2}{4\pi}\int d\mathbf{z}\frac{(1-\lambda)^{-2}(\mathbf{x}, a; \mathbf{z}, b)}{|\mathbf{z}-\mathbf{y}|}, \tag{3}$$

with the matrix elements of λ given by $(1-\lambda)(\mathbf{x}, a; \mathbf{y}, b) = \delta_{ab}\delta^3(\mathbf{x}-\mathbf{y}) - gf_{acb}\boldsymbol{\nabla}_y(1/|\mathbf{x}-\mathbf{y}|)\mathbf{A}^c(\mathbf{y})$. The Faddeev-Popov (FP) operator, $(1-\lambda)$, determines the curvature of the gauge manifold specified by the FP determinant, $\mathcal{J} = \det(1-\lambda)$. Finally, the interaction between the heavy sources, H_{QQ}, is given by

$$H_{QQ} = \frac{1}{2}\int d\mathbf{x}d\mathbf{y}\rho_Q^a(\mathbf{x})K[\mathbf{A}](\mathbf{x}, a; \mathbf{y}, b)\rho_Q^b(\mathbf{y}). \tag{4}$$

The Coulomb kernel is a complicated function of the transverse gluon field. When H_{Qg} and H_{QQ} are expanded in powers of the coupling constant, g, they lead to an infinite series of terms proportional to powers of $\mathbf{A}$. The FP determinant also introduces additional interactions. All these interactions involving gluons in the Coulomb potential are responsible for binding constituent gluons to the quark sources.

A. Fock space basis

The problem at hand is to find the spectrum of H for a system containing a $q\bar{q}$ pair,

$$H|R, N\rangle = E_N(R)|R, N\rangle. \tag{5}$$

In the Schrödinger representation, the eigenstates can be written as

$$|R, N\rangle = \int D[\mathbf{A}^a(x)]\mathcal{J}[A]\Psi^N_{ij}[\mathbf{A}^a(\mathbf{x})] \times \left|\frac{R}{2}\hat{\mathbf{z}}, i, -\frac{R}{2}\hat{\mathbf{z}}, j; \mathbf{A}\right\rangle, \tag{6}$$

with

$$\left|\frac{R}{2}\hat{\mathbf{z}}, i - \frac{R}{2}\hat{\mathbf{z}}, j; \mathbf{A}\right\rangle = h^\dagger_i\left(\frac{R}{2}\hat{\mathbf{z}}\right)\eta^\dagger_j\left(-\frac{R}{2}\hat{\mathbf{z}}\right)|\mathbf{A}\rangle \tag{7}$$

describing a state containing a quark at position $R\hat{\mathbf{z}}/2$ and color i and an antiquark at position $-R\hat{\mathbf{z}}/2$ and color j. We keep quark spin degrees of freedom implicit since, for static quarks, the Hamiltonian is spin independent. The eigenenergies, $E_N(R)$, correspond to the adiabatic potentials discussed in Sec. I with N labeling consecutive excitations and spin parity, Λ^Y_{PC}, quantum numbers of the gluons in the static $q\bar{q}$ state.

The vacuum without sources, denoted by $|0\rangle$, in the Schrödinger representation is given by

$$|0\rangle = \int D[\mathbf{A}^a(\mathbf{x})]\mathcal{J}[A]\Psi_0[\mathbf{A}^a(\mathbf{x})]|\mathbf{A}\rangle, \tag{8}$$

and satisfies $H_0|0\rangle = E_{\text{vac}}|0\rangle$.

The eigenenergies, $E_N(R)$, in Eq. (5) contain contributions from disconnected diagrams which sum up to the energy of the vacuum, E_{vac}. In the following, we will focus on the difference, $E_N(R) \to E_N(R) - E_{\text{vac}}$, and ignore disconnected contributions in the matrix elements of H.

Instead of using the Schrödinger representation, it is convenient to introduce a Fock space for quasiparticle-like gluons [26–29]. These are defined in the standard way, as excitations built from a Gaussian (harmonic oscillator) ground state. Regardless of the choice of parameters of such a Gaussian ground state, the set of all quasiparticle excitations forms a complete basis. We will optimize this basis by minimizing the expectation value of the Hamiltonian in such a Gaussian ground state. We will then use this variational state to represent the physical vacuum and use it in place of $|0\rangle$ and $\Psi_0[\mathbf{A}]$. The unnormalized variational wave functional is given by $\Psi_0[\mathbf{A}] = \langle\mathbf{A}|0\rangle$,

$$\Psi_0[\mathbf{A}] = \exp\left(-\frac{1}{2}\int\frac{d\mathbf{k}}{(2\pi)^3}\mathbf{A}^a(\mathbf{k})\omega(|\mathbf{k}|)\mathbf{A}^a(-\mathbf{k})\right), \tag{9}$$

where $\mathbf{A}^a(\mathbf{k}) = \int d\mathbf{x}\exp(-i\mathbf{k}\cdot\mathbf{x})\mathbf{A}^a(\mathbf{x})$ and the gap function, $\omega(|\mathbf{k}|)$ plays the role of the variation parameter. The computation of the expectation value of H_0 in Ψ_0 given above was described in Ref. [29]. In the following we will summarize the main points.

The expectation value of $\langle 0|H_0|0\rangle$ can be written in terms of functional integrals over $D[\mathbf{A}^a(\mathbf{x})]$ with the measure $\mathcal{J}[A]$. The functionals to be integrated are products of $H_0 = H_0(\Pi, \mathbf{A})$ and the wave functional $|\Psi_0[\mathbf{A}]|^2$. For example the contribution to $\langle 0|H_0|0\rangle$ from the $g = 0$ component of the transverse chromomagnetic field density, $\langle B^2\rangle = \langle 0|\int d\mathbf{x}[\mathbf{B}^a(\mathbf{x})]^2|0\rangle/\langle 0|0\rangle$, is given by

$$\langle B^2\rangle = \int D\mathbf{A}\mathcal{J}[\mathbf{A}][\boldsymbol{\nabla}\times\mathbf{A}^a(\mathbf{x})]^2\frac{\Psi_0^2[\mathbf{A}]}{\langle 0|0\rangle} = \mathcal{N}\int\frac{d\mathbf{k}}{(2\pi)^3}\frac{\mathbf{k}^2}{2\Omega(|\mathbf{k}|)}, \tag{10}$$

where $\mathcal{N} = 2\times(N_c^2 - 1)\times\mathcal{V}$ counts the total (infinite) number of gluon degrees of freedom in volume $\mathcal{V}$ and Ω is the instantaneous gluon-gluon correlation function,

$$\int D\mathbf{A}\mathcal{J}[\mathbf{A}]\mathbf{A}^a(\mathbf{p})\mathbf{A}^b(\mathbf{q})\frac{\Psi_0^2[\mathbf{A}]}{\langle 0|0\rangle} = \frac{\delta_{ab}}{2\Omega(|\mathbf{p}|)}(2\pi)^3\delta(\mathbf{p}+\mathbf{q}). \tag{11}$$

In the limit $\mathcal{J}\to 1$, Ω becomes equal to the gap function ω [26,28]. Evaluation of functional integrals over non-Gaussian distributions like the one in Eq. (11) for $\mathcal{J}\neq 1$ can be performed to the leading order in N_C by summing all planar diagrams. This produces a set of coupled integral (Dyson) equations for functions like $\Omega(p)$. The Dyson equations contain, in general, UV divergencies. To illustrate how renormalization takes place, let us consider an expectation value of the inverse of the FP operator,

$$\delta_{ab}d(\mathbf{x}-\mathbf{y}) \equiv \int D\mathbf{A}\mathcal{J}[\mathbf{A}]g(1-\lambda)^{-1}(\mathbf{x}, a; \mathbf{y}, b)\frac{\Psi_0^2[\mathbf{A}]}{\langle 0|0\rangle}. \tag{12}$$

From translational invariance of the vacuum, it follows that the integral depends on $\mathbf{x}-\mathbf{y}$ and the Dyson equation for d becomes simple in momentum space. Defining $d(\mathbf{x}-\mathbf{y})\to d(\mathbf{p}) = \int d\mathbf{x}\exp(-i\mathbf{k}\cdot\mathbf{x})d(\mathbf{x})$, one obtains ($p = |\mathbf{p}|$, etc.)

$$\frac{1}{d(p)} = \frac{1}{g(\Lambda)} - \frac{N_C}{2}\int^\Lambda\frac{d\mathbf{q}}{(2\pi)^3}\frac{(1-\hat{\mathbf{q}}\cdot\hat{\mathbf{p}})}{\Omega(|\mathbf{p}-\mathbf{q}|)\mathbf{q}^2}d(q). \tag{13}$$

As expected from asymptotic freedom, for large momenta, $\Omega(k)/k\to 1 + O(\log k)$; the integral in Eq. (12) becomes divergent as $q\to\infty$, and we need to introduce an UV cutoff Λ. The cutoff dependence can, however, be removed by renormalizing the coupling constant $g\to g(\Lambda)$. The final equation for $d(p)$, renormalized at a finite scale μ, is obtained by subtracting from Eq. (12) the same equation evaluated at $p = \mu$.

One also finds that the expectation value of $(1-\lambda)^2$, which enters in the Coulomb kernel, $K[\mathbf{A}]$, requires a

multiplicative renormalization. We define the Coulomb potential as

$$\int D\mathbf{A}\mathcal{J}[\mathbf{A}]K[\mathbf{A}](\mathbf{x}, a; \mathbf{y}, b)\frac{\Psi_0^2[\mathbf{A}]}{\langle 0|0\rangle} \equiv -\delta_{ab}V_C(\mathbf{x}-\mathbf{y}), \tag{14}$$

and introduce a function f by

$$V_C(k) = \int d\mathbf{x}e^{i\mathbf{k}\cdot\mathbf{x}}V_C(\mathbf{x}) \equiv -\frac{f(k)d^2(k)}{k^2}. \tag{15}$$

This function then satisfies a renormalized Dyson equation,

$$f(k) = f(\mu) + \left[\frac{N_C}{2}\int\frac{d\mathbf{q}}{(2\pi)^3}\frac{(1-\hat{\mathbf{q}}\cdot\hat{\mathbf{p}})d^2(q)f(q)}{\Omega(|\mathbf{p}-\mathbf{q}|)\mathbf{q}^2} - (k\rightarrow\mu)\right]. \tag{16}$$

Finally, the bare gap equation, $\delta[\langle 0|H_0|0\rangle/\langle 0|0\rangle]/\delta\omega(k) = 0$, contains a quadratic divergence proportional to $\sim\Lambda^2$. This divergence is eliminated by a single relevant operator from the regularized Hamiltonian, the gluon mass term, which is proportional to $\Lambda^2\int d\mathbf{x}\mathbf{A}^a(\mathbf{x})$. The renormalized gap equation determines the gap function $\omega(k)$, and it depends on a single dimensional subtraction constant, $\omega(\mu)$.

The functions described above completely specify the variational ground state, and the complete Fock space basis can be constructed by applying to this variational ground state quasiparticle creation operators, $\alpha^{a,\dagger}(\mathbf{k}, \lambda)$, defined by

$$\begin{aligned}\mathbf{A}^a(\mathbf{x}) &= \int\frac{d\mathbf{k}}{(2\pi)^3}\frac{1}{\sqrt{2\omega(k)}}[\alpha^a(\mathbf{k}, \lambda)\boldsymbol{\epsilon}(\mathbf{k}, \lambda) + \alpha^{a,\dagger}(-\mathbf{k}, \lambda)\boldsymbol{\epsilon}(-\mathbf{k}, \lambda)]e^{i\mathbf{k}\cdot\mathbf{x}},\\ \Pi^a(\mathbf{x}) &= -i\int\frac{d\mathbf{k}}{(2\pi)^3}\sqrt{\frac{\omega(k)}{2}}[\alpha^a(\mathbf{k}, \lambda)\boldsymbol{\epsilon}(\mathbf{k}, \lambda) - \alpha^{a,\dagger}(-\mathbf{k}, \lambda)\boldsymbol{\epsilon}(-\mathbf{k}, \lambda)]e^{i\mathbf{k}\cdot\mathbf{x}}.\end{aligned} \tag{17}$$

Here $\boldsymbol{\epsilon}$ represent helicity vectors with $\lambda = \pm 1$. This Fock space and the corresponding Hamiltonian matrix elements depend on four parameters (renormalization constants), $\omega(\mu)$, $d(\mu)$, $f(\mu)$ and one constant needed to regulate the FP determinant. The FP determinant enters into the Dyson equation for $\Omega(k)$.

In principle, if the entire Fock space is used in building the Hamiltonian matrix and no approximations are made in diagonalization, the physical spectrum will depend on the single parameter of the theory i.e. the renormalized coupling [or $d(\mu)$, cf. Eq. (13)]. In practical calculations, the Fock space is truncated and this may introduce other renormalization constants. Goodness of a particular basis, for example, the one built on the state given in Eq. (9), can be assessed by studying sensitivity of physical observables to these residual parameters.

For example, if we define the running coupling as $\alpha(k) \equiv f(k)d^2(k)$, so that $V_C(k) = -4\pi\alpha(k)/k^2$, we will find that for large k, $\alpha(k) \propto (1/\log^c(k))[1 + O(1/\log(k))]$ where $c \sim 1.5$, [29], while in full QCD the leading log has power $c = 1$. The discrepancy arises because we used the single Fock state, $|0\rangle$ in definition of V_C (and α). This omits, for example, the contribution from the two-gluon Fock state, as shown in Fig. 1. This two-gluon intermediate state clearly impacts the short range behavior of the Coulomb interaction, but, as discussed in [29], it is not expected to affect the long-range part (partially because the low momentum gluons develop a large constituent mass). Similarly, in [28], the role of the FP determinant has been analyzed, and it was shown that it does not make a quantitative difference leading to $\Omega(p) \sim \omega(p)$.

This is in contrast, however, to the results of [27]. We think this discrepancy originates from the difference in the boundary conditions which in [27] lead to $f(k) = 1$. This makes possible for the gap equation to have a solution for $\omega(k)$ which rises at low momenta. If $f(k) \neq 1$ and, in particular, if $f(k)$ grows as $k \rightarrow 0$, which is necessary if $V_C(R)$ is to grow linearly for large R, we find that $\omega(k)$ has to be finite as $k \rightarrow 0$. A more quantitative comparison is currently being pursued. We also note that lattice simulations [30] are consistent with the results of [28,29].

In the following, we will thus set $\mathcal{J} = 1$, which makes $\Omega = \omega$, and use the solutions for $f(k)$, $d(k)$ and $\omega(k)$ found in Ref. [29].

Finally, we want to stress that the Coulomb potential, defined in Eqs. (14) and (15), gives the energy expectation value in the state obtained by adding the $q\bar{q}$ pair to the vacuum of Eqs. (8) and (9), i.e.,

$$\langle q\bar{q}|H|q\bar{q}\rangle = C_F V_C(R) - C_F V_C(0), \tag{18}$$

with $C_F V_C(0)$ originating from self-energies, and

$$|q\bar{q}\rangle = |R, N = 0, \Sigma_g^+\rangle = \frac{1}{\sqrt{N_C}}h^\dagger\left(\frac{R}{2}\hat{\mathbf{z}}\right)\eta^\dagger\left(-\frac{R}{2}\hat{\mathbf{z}}\right)\frac{|0\rangle}{\langle 0|0\rangle}. \tag{19}$$

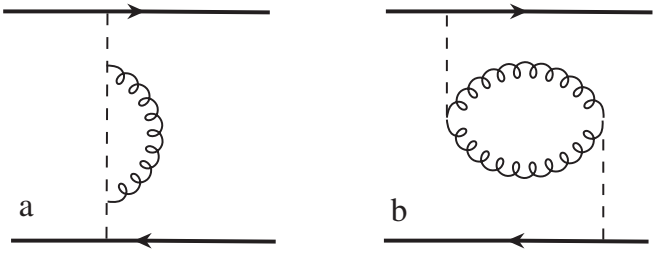

FIG. 1. The $O(g^4)$, one loop diagrams contributing to the leading log term in the expansion of the β function in YM theory with heavy sources. (a) Antiscreening dressing of the Coulomb potential by transverse gluons, (b) Debye screening of the Coulomb potential by transverse gluons. The Coulomb potentials are represented by the dashed lines, and sources by thick lines.

The state $|R, N = 0, \Sigma_g^+\rangle$ refers to the ground state ($N = 0$) with spin-parity quantum numbers $\Lambda_{PC}^Y = 0(\Sigma)_g^+$. The energy $C_F V_C(R)$ should be distinguished from $E_0(R)$ in Eq. (5). The latter is evaluated using the *true* ground state of the $q\bar{q}$ system while the former is evaluated in a state obtained by simply adding a $q\bar{q}$ pair to the vacuum. Since a $q\bar{q}$ pair is expected to polarize the gluon distribution, these two states are different. Furthermore, in this work, the $|q\bar{q}\rangle$ state in Eq. (19) is obtained by adding the $q\bar{q}$ pair to the *variational* state of the vacuum and not to the true vacuum state in the absence of sources.

B. Fitting the Coulomb potential

As discussed above, the Coulomb energy, $C_F V_C(R)$, represents the expectation value of the Hamiltonian in a particular $q\bar{q}$ state [given in Eq. (19)], which is not the same as the true eigenstate of the Hamiltonian for the $q\bar{q}$ system as defined in Eq. (5). The latter has energy $E_0(R)$.

According to [23], $C_F V_C(R) > E_0(R)$ and numerical results in [22] further indicate that for large R, $C_F V_C(R) \sim \sigma_C R$ and $E_0(R) \sim \sigma R$ with the Coulomb string tension, σ_C, being approximately 3 times larger than σ. In [29] we, however, fitted $d(\mu)$, $f(\mu)$ and $\omega(\mu)$ so that $C_F V_C(R) \rightarrow E_0(R)$, and a number of phenomenological studies have been successful with those parameters [31–34]. It should be noted, however, that the results from [22] for $C_F V_C(R)$ may not directly apply to our analysis since the $q\bar{q}$ state used here to define $V_C(R)$ may be different from the one used in lattice computations of $V_C(R)$. Guided by the successes of the phenomenological applications of our approach we proceed with fitting $C_F V_C(R)$ to $E_0(R)$. It is clear, however, that since the $q\bar{q}$ state of Eq. (19) is a variational state, $C_F V(R)$ should be greater than $E_0(R)$ [23]. We will nevertheless proceed with the approximation $C_F V_C(R) = E_0(R)$ and examine the consequences afterwards.

In [29], we have found that the numerical solutions to the set of coupled Dyson equations for $d(k)$, $f(k)$ and $\omega(k)$ can be well represented by

$$d(k) = \begin{cases} 3.5\left(\frac{m_g}{k}\right)^{0.48} & \text{for } k < m_g, \\ 3.5\left(\frac{\log(2.41)}{\log(k^2/m_g^2+1.41)}\right)^{0.4} & \text{for } k > m_g, \end{cases} \tag{20}$$

$$f(k) = \begin{cases} 1.41\left(\frac{m_g}{k}\right)^{0.97} & \text{for } k < m_g, \\ 1.41\left(\frac{\log(1.82)}{\log(k^2/m_g^2+0.82)}\right)^{0.62} & \text{for } k > m_g, \end{cases} \tag{21}$$

$$\omega(k) = \begin{cases} m_g & \text{for } k < m_g, \\ k & \text{for } k > m_g. \end{cases} \tag{22}$$

The parameter $m_g = 650$ MeV effectively represents the constituent gluon mass. It should be noticed, however, that $\omega(k)$ is the gap function and not the single quasiparticle energy. This energy, denoted by $E_g(k)$ is given by

$$E_g(k) = \omega(k)\left[1 - \frac{N_C}{2}\int \frac{d\mathbf{q}}{(2\pi)^3} V_C(\mathbf{k}-\mathbf{q}) \frac{1 + \hat{\mathbf{k}}\cdot\hat{\mathbf{q}}}{2\omega(q)}\right]. \tag{23}$$

Since $V_C(k) = -f(k)d^2(k)/k^2$, which for small k grows faster then k^3, the integral in Eq. (23) is divergent. This IR divergence is a manifestation of the long-range nature of the confining Coulomb potential which removes single, colored excitations from the spectrum. As will be explicit in the examples studied later, residual interactions between colored constituents in color neutral states cancel such divergencies and result in a finite spectrum for color neutral states. In the following analysis, we will also need the Coulomb potential in coordinate space. We find it practical to approximate the numerical Fourier transform of $V_C(\mathbf{k} - \mathbf{q})$ by

$$V_C(r) = br - \frac{\alpha}{r\log^c[(r\Lambda)^{-1} + a]}, \tag{24}$$

with $b = 0.20$ GeV^2, $\alpha = 0.83$, $\Lambda = 0.63$ GeV, $a = 1.24$ and $c = 1.51$. Comparison between $C_F V_C(R)$ and $E_0(R)$ obtained from lattice computations is shown in Fig. 2.

We now proceed to the main subject of this paper, namely, to investigate the difference between $E_0(R)$ computed using the single Fock space approximation to the $q\bar{q}$ state (i.e. without modification of the gluon distribution) and the solution of Eq. (5) which accounts for modifications in the gluon distribution in the vacuum in the presence of $q\bar{q}$ sources. We will also compute the first excited potential with the Σ_g^+ symmetry.

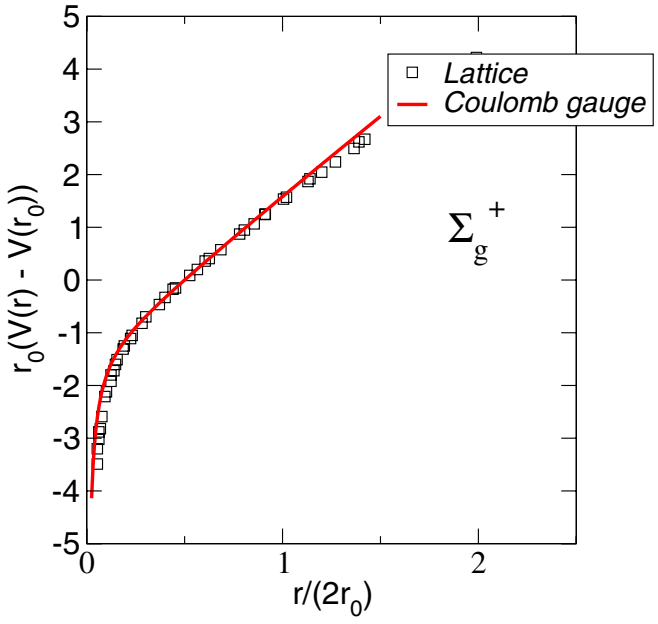

FIG. 2 (color online). Comparison between $V(R) = C_F V_C(r)$ from Eq. (24) (solid line) and $V(R) = E_0(R)$ lattice data from [1] ($r_0 = 1/450$ MeV^{-1}).

III. ADIABATIC POTENTIALS

To diagonalize the full Hamiltonian in the Fock space described above, in principle, requires an infinite number of states. In the zeroth-order approximation, $E_0(R) = C_F V_C(R)$, a single state with no quasigluons was used. At vanishing $q\bar{q}$ separation, we expect the wave function of the system to be identical to that of the vacuum, and the approximation becomes exact. One also expects that the average number of quasigluon excitations in the full wave functional of Eq. (6) increases with the $q\bar{q}$ separation. We thus start by examining the approximation based on adding a single quasigluon and truncate the Hamiltonian matrix to a space containing $|q\bar{q}\rangle$ and $|q\bar{q}g\rangle$ states,

$$\begin{bmatrix} \langle q\bar{q}|Hq\bar{q}\rangle & \langle q\bar{q}|H|q\bar{q}g\rangle \\ \langle q\bar{q}g|H|q\bar{q}\rangle & \langle q\bar{q}g|H|q\bar{q}g\rangle \end{bmatrix} \begin{bmatrix} |q\bar{q}\rangle \\ |q\bar{q}g\rangle \end{bmatrix} = E_N(R) \begin{bmatrix} |q\bar{q}\rangle \\ |q\bar{q}g\rangle \end{bmatrix}. \quad (25)$$

The $|q\bar{q}\rangle$ state is given in Eq. (19). In the quasiparticle representation the state with a single gluon and Λ^Y_{PC} quantum numbers, $|q\bar{q}g\rangle = |R, n, \Lambda^Y_{PC}\rangle$ is given by

$$|R, N, \Lambda^Y_{PC}\rangle = \sum_{j_g,\xi,\mu,\lambda} \sqrt{\frac{2j+1}{8\pi C_F N_C}} \int \frac{d\mathbf{k}}{(2\pi)^3} [D^{j_g *}_{\Lambda\mu}(\hat{\mathbf{k}}) + \eta_Y D^{j_g *}_{-\Lambda\mu}(\hat{\mathbf{k}})] \psi^{j_g}_N(k) \chi^{\xi}_{\mu\lambda} |R, \mathbf{k}, \lambda\rangle, \quad (26)$$

for $\Lambda \neq 0$ and

$$|R, N, 0^{PC}_Y\rangle = \sum_{j_g,\xi,\mu,\lambda} \sqrt{\frac{2j+1}{4\pi C_F N_C}} \int \frac{d\mathbf{k}}{(2\pi)^3} D^{j_g *}_{0\mu}(\hat{\mathbf{k}}) \times \psi^{j_g}_N(k) \chi^{\xi}_{\mu\lambda} |R, \mathbf{k}, \lambda\rangle, \quad (27)$$

for $\Lambda = 0$ (Σ potentials) where

$$|R, \mathbf{k}, \lambda\rangle = h^\dagger\left(\frac{R}{2}\hat{\mathbf{z}}\right) \alpha^\dagger(\mathbf{k}, \lambda) \eta^\dagger\left(-\frac{R}{2}\hat{\mathbf{z}}\right) \frac{|0\rangle}{\langle 0|0\rangle}, \quad (28)$$

and $\alpha^\dagger = \alpha^{a,\dagger} T^a$. In Eqs. (26) and (27), j_g is the total angular momentum of the quasigluon. For vanishing separation between the quarks, the system has full rotational symmetry, and j_g becomes a good quantum number. In general, the system is invariant only under rotations around the $q\bar{q}$ axis. It is only the projection of the total angular momentum, Λ, that is conserved and states with different j_g become mixed. The wave function $\chi^{\xi}_{\mu\lambda}$ represents the two possibilities for the spin-orbit coupling of given parity ($j_g = L_g$ or $j_g = L_g \pm 1$). It is given by $\delta_{\mu\lambda}/\sqrt{2}$ for $\xi = 1$ and $\lambda\delta_{\mu\lambda}/\sqrt{2}$ for $\xi = -1$, corresponding to TM (natural parity) and TE (unnatural parity) gluons, respectively. Finally η_Y determines the behavior under reflections in the plane containing the $q\bar{q}$ axis, i.e., the Y parity.

The radial wave functions, $\psi^{j_g}_N(k)$, labeled by the radial quantum number N and j_g, are obtained by diagonalizing the full Hamiltonian in the Fock space spanned by the $q\bar{q}g$ states alone, i.e. by solving the equation,

$$PHP|R, N, \Lambda^Y_{PC}\rangle = V^{qqg}_{C,N}(R)|R, N, \Lambda^Y_{PC}\rangle. \quad (29)$$

Here P projects on the $|q\bar{q}g\rangle$ state and $V^{qqg}_{C,N}(R)$ are the *bare* energies of the excited adiabatic potentials, i.e., without mixing between states with a different number of quasigluons. Analogously, $C_F V_C(R)$ is the bare ground state energy $E_0(R)$. The matrix elements of PHP are shown in Fig. 3 and given explicitly in the Appendix.

The mixing matrix element,

$$\langle q\bar{q}|H|q\bar{q}g\rangle = V^{qq,qqg}_{C,N}(R), \quad (30)$$

depends on the number of bare, $q\bar{q}g$ states from Eq. (29) kept, $N = 1, \ldots, N_{\max}$ and the separation between the sources, R. It is shown in Fig. 4 and given in the Appendix.

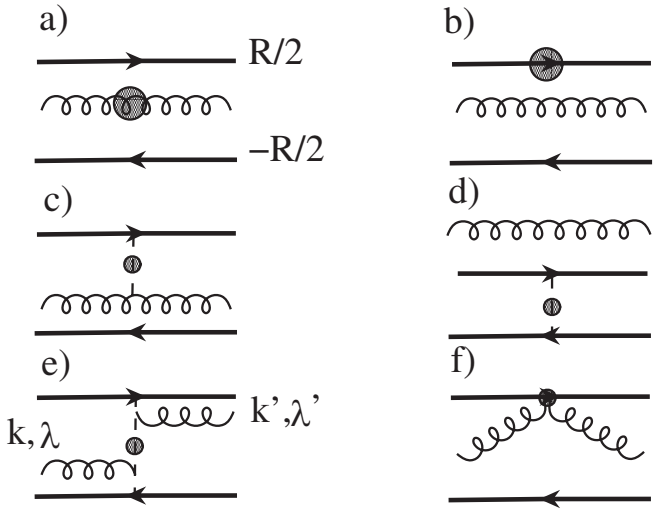

FIG. 3. Matrix elements, $\langle R, \mathbf{k}', \lambda'|H|R, \mathbf{k}, \lambda\rangle$. (a) and (b) represent gluon and quark self-energies, respectively. (c) and (d) represent the Coulomb interaction, V_C between the gluon and one of the quarks and between the two quarks, respectively. In the bottom row, (e) and (f) describe matrix elements of the interaction term resulting from expansion of the Coulomb kernel $K[A]$ in up to one power in gluon field. The short dashed vertical lines in (c)–(e) represent the dressed (blob) Coulomb potentials.

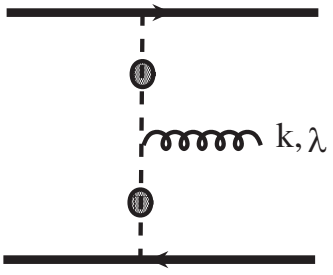

FIG. 4. The matrix element $\langle R|H|R, \mathbf{k}, \lambda\rangle$. It originates from expansion of the Coulomb kernel $K[A]$ to first order in A.

The $(N_{\max}+1)\times(N_{\max}+1)$ Hamiltonian matrix shown in Eq. (25) is explicitly given by

$$H_{NM}=\begin{cases} C_F[V_C(R)-V_C(0)] & N=M=0, \\ V_{C,M}^{qq,qqg}(R) & N=0, M=1-N_{\max}, \\ V_{C,N}^{qq,qqg*}(R) & N=1-N_{\max}, M=0, \\ V_{C,N}^{qqg}(R)\delta_{NM} & N,M=1-N_{\max}. \end{cases} \tag{31}$$

IV. NUMERICAL RESULTS

In terms of ξ and η, the PC and Y quantum numbers of the gluonic field are given by

$$PC=\xi(-1)^{j_g+1}, \qquad Y=\begin{cases} \xi\eta_Y(-1)^{\Lambda} & \text{for } \Lambda\neq 0, \\ \xi & \Lambda=0. \end{cases} \tag{32}$$

In the following, we will concentrate on the states with $\Lambda=0$, $PC=g(+)$ and $Y=+$, i.e., of Σ_g^+ symmetry, since it is only these states that mix the bare $|q\bar{q}\rangle$ state with the states with a nonvanishing number of gluons.

For the Σ_g^+ potentials, the wave function contains TM gluons, $\xi=1$ of natural parity and $PC=+1$ which implies $j_g=1,3,\ldots$. As discussed above, for $R\to 0$, j_g becomes a good quantum number, and we have verified numerically that for R in the range considered here the contributions from $j_g=3$ and higher are at a level of a few percent. Diagonalization of the Hamiltonian in the $q\bar{q}g$ subspace alone leads to the $V_{C,N}^{q\bar{q}g}(R)$ potential which is shown in Fig. 5 (upper solid line) for the lowest excitation with $N=1$. The dashed line is the result of using the one- and two-body interactions depicted in Figs. 3(a)–3(d). [H in Eq. (A2)]. These are also the interactions that were used in [17]. When the three-body interactions shown in Figs. 3(e) and 3(f) are added, the energy moves up. This discrepancy is then also a measure of how far our variational, truncated Fock space expansion is from the true excited state. The three-body potential is expected to be responsible for reversing the ordering between the Π_u and Π_g surfaces; with only one- and two-body interactions, the Π_g potential has lower energy than Π_u, which is inconsistent with the lattice data [17]. In the Appendix, we also show that the three-body term is suppressed at large separations, and thus the net potential approaches the Casimir scaling $C_F bR$ limit as $R\to\infty$. Finally, we note that when the Fock space is restricted to single quasigluon excitations, the diagrams in Figs. 3 and 4 represent the complete set of Hamiltonian matrix elements.

The general features of higher excitations, $V_{C,N}^{qqg}(R)$ for $N>1$, follow from the structure of the Hamiltonian, which represents a one-body Schrödinger equation for the single quasigluon wave function in momentum space. The kinetic energy corresponds to the one-body diagram in Fig. 3(a) and the potential to the diagrams in Figs. 3(c), 3(e), and 3(f). The diagrams in Figs. 3(b) and 3(d) give an R-dependent shift describing the $q\bar{q}$ self-interactions and $q\bar{q}$ octet potential. The IR singularity in the gluon kinetic energy, E_g, is canceled by the collinear singularity of the two-body potential, the $q\bar{q}$ self-energy and $q\bar{q}$ octet potential. On average, gluon kinetic energy contributes an effective quasigluon mass of the order of m_g. Quasigluons are thus heavy, and adding Fock space components, with more gluons, $|q\bar{q},2g\rangle,\ldots|q\bar{q}n_g g\rangle$, for small R will result in higher adiabatic potentials with $(N=2,3,\ldots)$ that are split from the first excited state by $\sim n_g m_g$. At large R, the two-body Coulomb potential dominates and together with Coulomb energies of the pairwise gluon interactions results in the Casimir scaling (we will discuss this in more detail in the following section). In the absence of mixing between Fock space components the number of quasiparticle gluons in the $|q\bar{q},n_g g\rangle$ state is conserved, and they directly map in to the tower of excited adiabatic potentials.

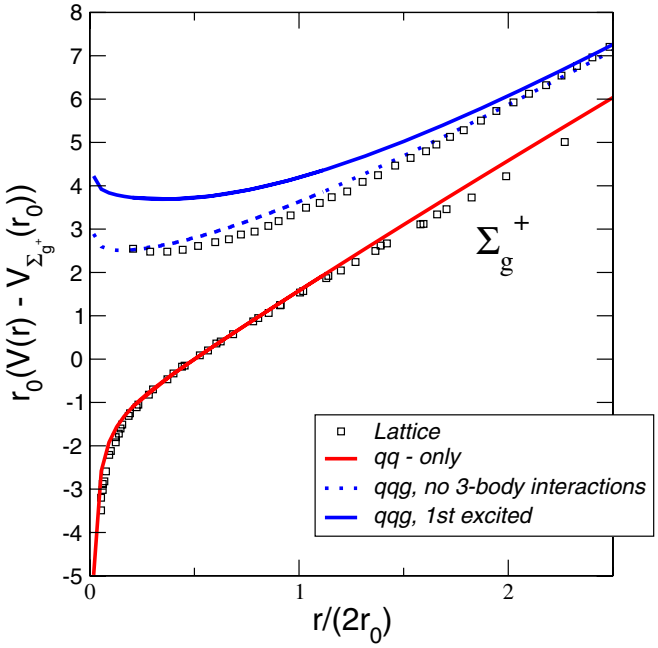

FIG. 5 (color online). Comparison between $V(R)=C_F V_C(r)$ from Eq. (24) (lower solid line) and the $V(R)=E_0(R)$ lattice data from [1] ($r_0=1/450$ MeV^{-1}). The upper solid line represents the first excited state.

We will now address the effects of mixing between $|q\bar{q}\rangle$ and $|q\bar{q}g\rangle$ states. The only nonvanishing diagram is shown in Fig. 4. Since, as discussed above, the $V_{C,N}^{qqg}(R)$ potentials are split from the first excited state, $N=1$, by at least m_g, the mixing matrix in Eq. (31) saturates quickly, and in practice, only the $N=1$ state is relevant. However, even this single state mixing leads to a very small energy shift. In Fig. 6 the dashed line corresponds to the energy of the ground state without mixing, (the same as the solid line in Fig. 5), and the solid line shows the effect of mixing. The effect of the mixing is small. Numerically, we find that the

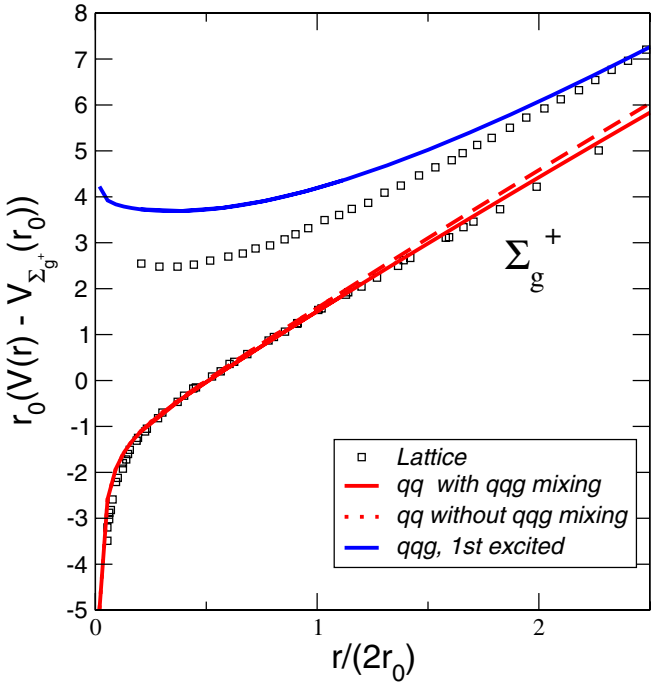

FIG. 6 (color online). Comparison between $V(R) = C_F V_C(r)$ from Eq. (24) (lower solid line) and the $V(R) = E_0(R)$ lattice data from [1] ($r_0 = 1/450$ MeV^{-1}). The (dashed) line labeled qq without qqg mixing is only slightly above the (lower solid) line labeled qq with qqg mixing. The upper solid line represents the first excited state. For the excited state the effect of mixing with the qqg component is even smaller than for the ground state and invisible on the scale of this graph.

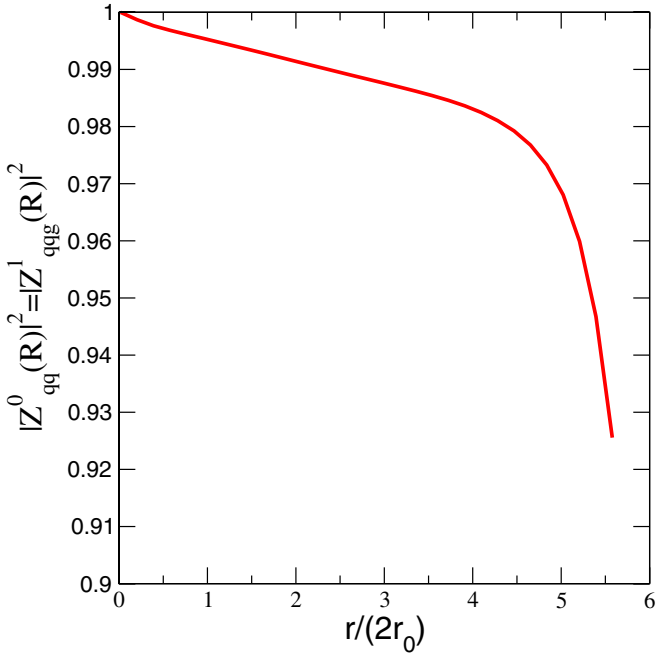

FIG. 7 (color online). Normalized probability of finding the bare $|q\bar{q}\rangle$ state in the full ground state of the $|qq, N = 0\rangle$ (which is also equal to the probability of finding the $|q\bar{q}g\rangle$ state in the first excited $|qq, N = 1\rangle$ state).

full ground state,

$$|q\bar{q}, N = 0\rangle = Z^0_{qq}(R)|q\bar{q}\rangle + Z^0_{qqg}|q\bar{q}g\rangle, \qquad (33)$$

is still dominated by the $|q\bar{q}\rangle$ component and the first excited state,

$$|q\bar{q}, N = 1\rangle = Z^1_{qq}(R)|q\bar{q}\rangle + Z^1_{qqg}|q\bar{q}g\rangle, \qquad (34)$$

by the $|q\bar{q}g\rangle$ component. The probabilities of each are shown in Fig. 7. We see that, for distances between sources as large as 5 fm, the admixture of the gluon component is only of the order of 10%.

This small admixture of the $|q\bar{q}, g\rangle$ in the full ground state is correlated with the small shift in the Σ_g^+ surface shown in Fig. 6 and would justify using the ground state, exact Σ_g^+ energy to constrain the Coulomb potential V_C. This is, however, contradicting the results of Ref. [21] where the effect of mixing must be large since it results in a factor of 3 in the ratio of the unmixed to mixed string tensions. One possible explanation is that there is an accidental suppression of the mixing interaction matrix element for the two states considered here, $|q\bar{q}\rangle$ and $|q\bar{q}g\rangle$. Inspecting Eq. (A14), we note that due to the gradient coupling of the transverse gluon to the Coulomb line, the coupling vanishes both for small and large R. In contrast, a two-gluon state can be coupled to $|q\bar{q}\rangle$ with either the Coulomb line mediated interaction as shown in Fig. 8(a) or the quark density–gluon density interaction shown in Fig. 8(b). As discussed in the Appendix, at large distances the former is suppressed and it is easy to show that the latter is proportional to $C_F V_C(\mathbf{x} - \mathbf{R}/2) + C_F V_C(\mathbf{x} + \mathbf{R}/2)$ (once the gluon spin is neglected) and persists at large distances. In the large-N_C limit $C_F = N_C/2(1 + O(1/N_C))$. It is therefore possible that the $|q\bar{q}, 2g\rangle$ component of the full $|q\bar{q}, N = 0\rangle$ state is actually more important then the $|q\bar{q}g\rangle$ one. We will investigate this further in Sec. IV A.

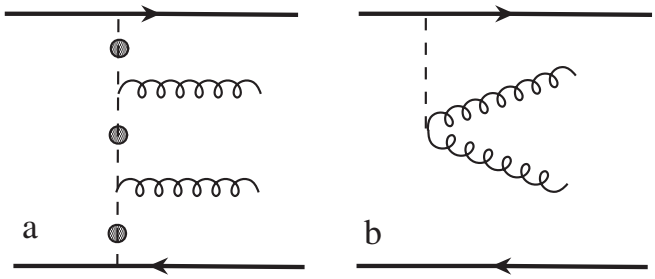

FIG. 8. Matrix elements $\langle qq|H|q\bar{q}, 2g\rangle$ leading to the $|q\bar{q}, 2g\rangle$ component in the ground state Σ_g^+ potential, (a) interaction mediated via the Coulomb line coupled to quark sources, (b) interaction between a single quark and the gluon charge density.

A. Multigluons states and the chain model

As shown above, the quasigluon degrees of freedom defined in terms of a variational quasiparticle vacuum provide an attractive basis for describing gluon excitations. This is in the sense that for source separations relevant for phenomenology the color singlet states can be effectively classified in terms of the number of quasigluons. This basis, however, does overestimate the energies (as expected in a variational approach), and this fact together with lessons from other models can give us guidance for how to improve on the variational state of the $q\bar{q}$ system. As the separation between quarks increases one expects the average number of gluons in the energy eigenstate to increase. This is because it becomes energetically favorable to add a constituent gluon which effectively screens the $q\bar{q}$ charge. Furthermore, the spacial distribution of these gluons is expected to be concentrated near the $q\bar{q}$ axis in order for the energy distribution to be that of a flux tube, as measured by the lattice. An improvement in the ansatz wave functional will therefore result in a more complicated Fock space decomposition with a large number of quasigluons present, even at relatively small separations between the sources. In this section we will first discuss how multigluon states indeed become important, even in the case of the quasigluon basis used here. We then compare with expectations from other models and discuss the possible directions for improving the quasigluon basis.

As discussed in the Appendix, at large separations the interactions between multigluon Fock states mediated by the Coulomb potential, shown in Figs. 9(a) and 9(b), require all but two gluons to be at relative separations smaller than R. Furthermore, rearrangement of gluons leads to $1/N_C$ suppression. For large R, the largest diagonal matrix elements of H are the ones corresponding to the long-range Coulomb interaction between charge densities as shown in Figs. 9(c) and 9(d). To leading order in N_C, the gluons should be path ordered along the $q\bar{q}$ axis. For simplicity, we will neglect the gluon spin and use a single wave function to represent a state with an arbitrary number of gluons. We write

$$|q\bar{q}, n_g g\rangle = N_{n_g} \int_{-R/2}^{R/2} dx_{n_g} \alpha^\dagger(x_{n_g}) \times \int_{-R/2}^{x_{n_g}} dx_{n_g-1} \alpha^\dagger(x_{n_g-1}) \cdots \int_{-R/2}^{x_3} dx_2 \alpha^\dagger(x_2) \times \int_{-R/2}^{x_2} dx_1 \alpha^\dagger(x_1)|0\rangle, \quad (35)$$

where we have also forced all gluons to be on the $q\bar{q}$ axis. The factor $N_{n_g} = (n_g!/C_F N_C R)^{1/2}$ is to leading order in N_C fixed by the normalization condition, $\langle q\bar{q}, n_g g|q\bar{q}, n'_g g\rangle = \delta_{n_g,n'_g}$, where we used $[\alpha(x_i), \alpha^\dagger(x_j)] = \delta_{ij}$. In this basis, the diagonal matrix elements of the Hamiltonian [cf. Figs. 9(c) and 9(d)] add up to

$$H_{n_g n'_g} = \langle q\bar{q}, n_g g|H|q\bar{q}, n'_g g\rangle = C_F V_C(R) \to C_F b R \delta_{n_g,n'_g}. \quad (36)$$

The off-diagonal matrix elements are dominated by interactions between color charges, e.g., similar to the ones in Fig. 8(b), but with the upper vertex attached to a gluon line. With the approximations leading to Eq. (35) a vertex which either annihilates or creates two gluons results in a vanishing matrix element since in our basis no two gluons are at the same point. Smearing each gluon in the coordinate space by a distance of the order of $1/m_g$ will give a finite matrix element, which just like the diagonal matrix elements grows linearly with R,

$$H_{n_g n'_g} = \langle q\bar{q}, n_g g|H|q\bar{q}, n'_g g\rangle \to \gamma C_F b R[\delta_{n_g,n'_g+2} + \delta_{n_g,n'_g+2}], \quad (37)$$

where γ is a parameter representing the effect of a smearing, and we expect $|\gamma| < O(1)$. In addition, each gluon has a kinetic energy of the order of m_g, so $H_{nn} \to H_{nn} + n m_g$. The model Hamiltonian can be easily diagonalized numerically, and in Fig. 10, we plot the energy of the ground state and of the first excited state as a function of R. It is clear that in the absence of accidental spin suppression, which, as discussed earlier, takes place for the $\langle q\bar{q}|H|q\bar{q}g\rangle$ mixing matrix, the effect of the mixing with two and more gluons can produce shifts in the lowest adiabatic potential and decrease the Coulomb string tension by as much as a factor of ~ 2 at $R \sim 3r_0 = 2.6$ fm. Finally, in Fig. 11 we plot the average number of gluons in the ground state of the

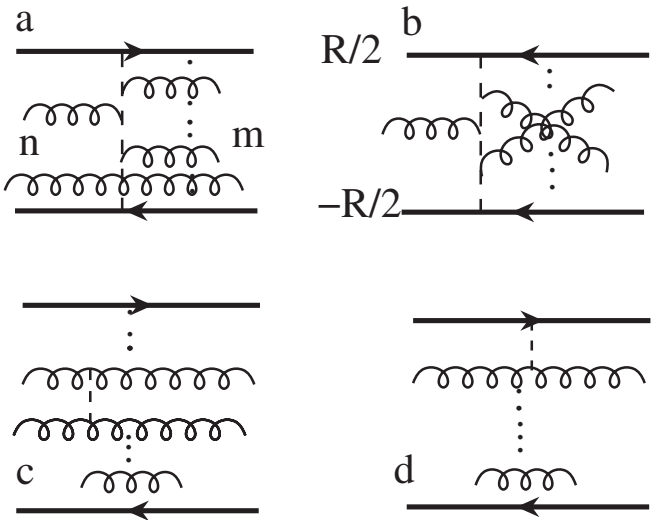

FIG. 9. Typical diagrams contribution to mixing between n and m gluon states. Vertical dots represent any number of gluons not affected by the interaction. (a) mixing mediated by the Coulomb potential, (b) same as in (a) with the rearrangement of gluons, (c) long-range Coulomb interaction between gluon charge densities, (d) same as in (c) but with the charge density of the quark sources.

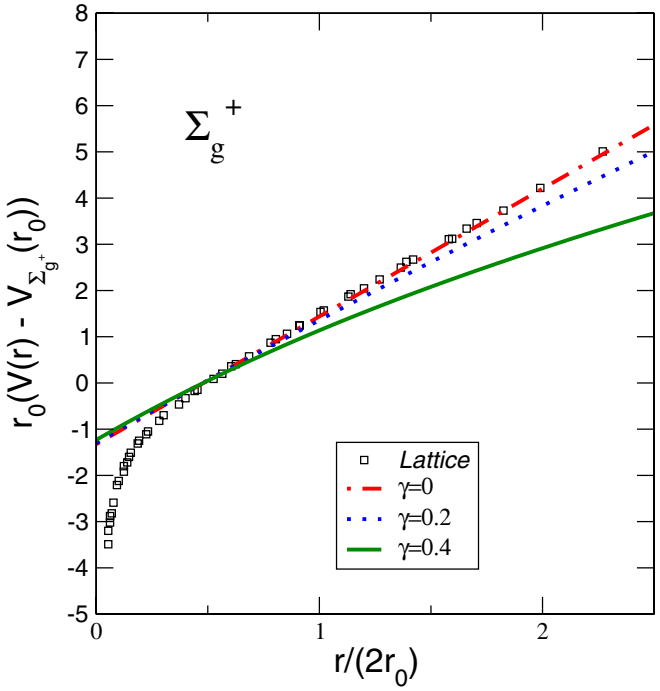

FIG. 10 (color online). Shift in the ground state Σ_g^+ energy due to coupling with mutigluon states of the model Hamiltonian of Eqs. (36) and (37). The maximum number of states was taken to be $n_{g,\max} = 40$. The other parameters are $b = 0.21$ GeV^{-2} and $m_g = 0.65$ GeV.

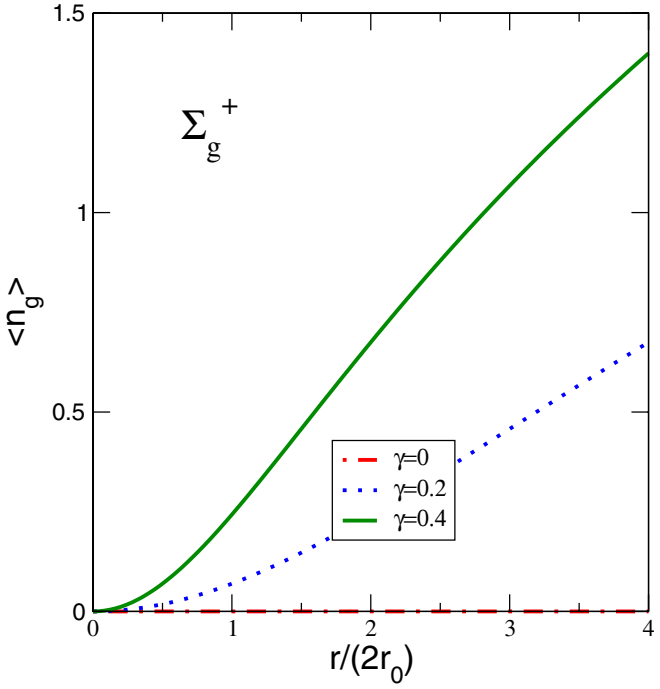

FIG. 11 (color online). Average number of quasigluons in the full eigenstate of the model Hamiltonian of Eqs. (36) and (37).

model Hamiltonian. As expected, the number of gluons grows with R; however, still a small number of quasigluons contributes to the ground state at these separations, which again provides justification for the quasigluon description.

V. SUMMARY AND OUTLOOK

We computed the ground state energy and the energy of the first excited $q\bar{q}$ potential with the $\Lambda_{PC}^Y = \Sigma_g^+$ symmetry. We used the quasiparticle basis of constituent gluons based on a variational ground state to build the Fock space representation. We found that the $q\bar{q}$ state can be well approximated by a superposition of the bare $q\bar{q}$ state and a few quasigluons. The exact computation in which the bare $q\bar{q}$ sate mixes with a state containing a single quasigluon leads to negligible change in the energy of the bare (Coulomb) $q\bar{q}$ system. We found that this is due to an accidental small mixing matrix element of the Coulomb gauge Hamiltonian. We have discussed the general properties of the mixing matrix between states with an arbitrary number of gluons, and using a simple approximation, we have found a good agreement with the lattice data. The lattice data indicate that there is a change in slope between the Coulomb and the true, Wilson potential [21]. Based on the representation used here, we interpret this in terms of quasigluon excitations rather than in terms of a flux-tube-like degrees of freedom. We also note that lattice data on splitting between several excited $q\bar{q}$ states do not unambiguously show a stringlike behavior for separation as large as 2–3 fm [2]. In fact, the splittings are almost constant, although why lattice data have such a behavior is not completely understood (including a possible systematic error) [35]. In fact these data are consistent with the quasigluon picture where each quasiparticle adds kinetic energy of the order of the effective gluon mass. The full excitation spectrum as well as distribution of energy density is currently being investigated.

ACKNOWLEDGMENTS

I would like to thank J. Greensite, C. Morningstar and E. Swanson, for several discussions and C. Halkyard for reading the manuscript. This work was supported in part by the U.S. Department of Energy grant under Contract No. DE-FG0287ER40365.

APPENDIX

Here we list matrix elements of the Hamiltonian in the basis spanned by $|q\bar{q}\rangle = |R, N = 0, \Lambda_{PC}^Y\rangle$ and $|q\bar{q}g\rangle = |R, N \neq 0, \Lambda_{PC}^Y\rangle$. The $|q\bar{q}\rangle$ state exists only in the $\Lambda_{PC}^Y = \Sigma_g^+$ configuration. Thus mixing matrix elements are nonvanishing for $|q\bar{q}g\rangle$ with Σ_g^+ spin-parity quantum numbers only.

For each j_g, the wave functions $\psi_{N,j_g}(k)$ are expanded in a complete orthonormal basis of functions $\phi_{m,j_g}(k)$

$$\psi_{N,j_g}(k) = \sum_{m=1}^{m_{\max}} a^m_{N,j_g} \phi_{m,j_g}(k) \tag{A1}$$

with normalization, $\int [dkk^2/(2\pi)^3] \phi^*_{m',j'_g}(k)\phi_{m,j_g}(k) = \delta_{m',m}\delta_{j'_g,j_g}$. The expansion coefficients are computed by diagonalizing the $(m_{\max} j_{g,\max}) \times (m_{\max} j_{g,\max})$ matrix, $\tilde{H}_{m'j'_g;m,j_g}$, obtained by evaluating the diagrams in Fig. 3,

$$\tilde{H}_3 = H_{3a} + H_{3b} + \cdots + H_{3f}, \tag{A2}$$

evaluated in the basis of functions ϕ_{m,j_g}. In numerical computations for each j_g, we used a momentum grid as the basis functions. The numerical results presented were for a single j_g determined from Eq. (32) after verifying that increasing j_g changes the computed spectrum by at most a few percent. For arbitrary Λ^Y_{PC} the Hamiltonian matrix elements are given by

$$H_{3a} = \frac{\delta_{j'_g,j_g}}{2} \int \frac{dkk^2}{(2\pi)^3} \phi^*_{m',j_g}(k) E_g(k) \phi_{m,j_g}(k), \tag{A3}$$

$$\begin{aligned} H_{3b} &= -C_F V_C(0) \delta_{m',m}\delta_{j'_g,j_g} \\ &= -4\pi C_F \int \frac{dkk^2}{(2\pi)^3} V_C(k) \delta_{m',m}\delta_{j'_g,j_g}, \end{aligned} \tag{A4}$$

with

$$V_C(k) = -\frac{d^2(k) f(k)}{k^2}, \tag{A5}$$

$$\begin{aligned} H_{3c} &= \frac{N_C}{2} \sum_{\lambda,\lambda',\sigma,\sigma',\mu} \int \frac{d\mathbf{q}}{(2\pi)^3} \int \frac{d\mathbf{k}}{(2\pi)^3} \phi^*_{m',j'_g}(q)\phi_{m,j_g}(k) \int d\mathbf{x} \left[V_C\left(\mathbf{x} - \frac{\mathbf{R}}{2}\right) + V_C\left(\mathbf{x} + \frac{\mathbf{R}}{2}\right)\right] e^{i\mathbf{x}\cdot(\mathbf{k}-\mathbf{q})} \frac{\sqrt{(2j'_g+1)(2j_g+1)}}{16\pi} \\ &\times [D^{j'_g}_{\Lambda,\sigma'}(\hat{\mathbf{q}}) D^{j_g,*}_{\Lambda\lambda'}(\hat{\mathbf{k}}) \chi^{\xi'}_{\sigma\sigma'} \chi^{\xi}_{\lambda\lambda'} D^{1*}_{\mu\sigma}(\hat{\mathbf{q}}) D^1_{\mu\lambda}(\hat{\mathbf{k}}) + \eta_Y \eta'_Y(\Lambda \to -\Lambda)] \left(\sqrt{\frac{\omega(k)}{\omega(q)}} + \sqrt{\frac{\omega(q)}{\omega(k)}} \right) \\ &= \frac{N_C}{2} \sum_{\lambda,\lambda',\sigma,\sigma',\mu} \int \frac{d\mathbf{q}}{(2\pi)^3} \int \frac{d\mathbf{k}}{(2\pi)^3} \phi^*_{m',j'_g}(q) V_C(\mathbf{k}-\mathbf{q}) [e^{-i(\mathbf{R}/2)\cdot(\mathbf{k}-\mathbf{q})} + e^{i(\mathbf{R}/2)\cdot(\mathbf{k}-\mathbf{q})}] \phi_{m,j_g}(k) \frac{\sqrt{(2j'_g+1)(2j_g+1)}}{16\pi} \\ &\times [D^{j'_g}_{\Lambda,\sigma'}(\hat{\mathbf{q}}) D^{j_g,*}_{\Lambda\lambda'}(\hat{\mathbf{k}}) \chi^{\xi'}_{\sigma\sigma'} \chi^{\xi}_{\lambda\lambda'} D^{1*}_{\mu\sigma}(\hat{\mathbf{q}}) D^1_{\mu\lambda}(\hat{\mathbf{k}}) + \eta_Y \eta'_Y(\Lambda \to -\Lambda)] \left(\sqrt{\frac{\omega(k)}{\omega(q)}} + \sqrt{\frac{\omega(q)}{\omega(k)}} \right), \end{aligned} \tag{A6}$$

and η_Y and ξ related to j_g and Λ^Y_{PC} through Eq. (32).

$$H_{3d} = -\frac{1}{2N_C} V_C(R) \delta_{m',m}\delta_{j'_g,j_g} = -4\pi \frac{1}{2N_C} \int \frac{dkk^2}{(2\pi)^3} V_C(k) j_0(Rk) \delta_{m',m}\delta_{j'_g,j_g}, \tag{A7}$$

$$\begin{aligned} H_{3e} &= \sum \int \frac{d\mathbf{k}}{(2\pi)^3} \frac{d\mathbf{p}}{(2\pi)^3} \frac{d\mathbf{q}}{(2\pi)^3} \frac{\phi^*_{m',j'_g}(p)}{\sqrt{2\omega(p)}} \frac{\phi_{m,j_g}(k)}{\sqrt{2\omega(k)}} \int d\mathbf{x} d\mathbf{y} d\mathbf{z} \left[K\left(\mathbf{x} - \frac{\mathbf{R}}{2}, \mathbf{z} + \mathbf{y} - \mathbf{x}, \mathbf{y} + \frac{\mathbf{R}}{2}\right) + (\mathbf{R} \to -\mathbf{R}) \right] \\ &\times e^{i\mathbf{x}\cdot\mathbf{k}} e^{i\mathbf{z}\cdot\mathbf{q}} e^{-i\mathbf{y}\cdot\mathbf{p}} \frac{\sqrt{(2j'_g+1)(2j_g+1)}}{8\pi} [D^{j'_g}_{\Lambda,\sigma'}(\hat{\mathbf{p}}) D^{1,*}_{\mu,\sigma}(\hat{\mathbf{p}}) \chi^{\xi'}_{\sigma'\sigma} D^1_{\mu,0}(\hat{\mathbf{q}}) D^{j_g,*}_{\Lambda,\lambda'}(\hat{\mathbf{k}}) D^1_{\nu,\lambda}(\hat{\mathbf{k}}) \chi^{\xi}_{\lambda'\lambda} D^{1,*}_{\nu,0}(\hat{\mathbf{q}}) \\ &+ \eta_Y \eta'_Y(\Lambda \to -\Lambda)] \\ &= \sum \int \frac{d\mathbf{k}}{(2\pi)^3} \frac{d\mathbf{p}}{(2\pi)^3} \frac{d\mathbf{q}}{(2\pi)^3} \frac{\phi^*_{m',j'_g}(p)}{\sqrt{2\omega(p)}} \frac{\phi_{m,j_g}(k)}{\sqrt{2\omega(k)}} K(\mathbf{k}+\mathbf{q}, \mathbf{q}, \mathbf{p}+\mathbf{q}) [e^{i(\mathbf{R}/2)\cdot(\mathbf{k}+\mathbf{p}+2\mathbf{q})} + (\mathbf{R} \to -\mathbf{R})] \\ &\times \frac{\sqrt{(2j'_g+1)(2j_g+1)}}{8\pi} [D^{j'_g}_{\Lambda,\sigma'}(\hat{\mathbf{p}}) D^{1,*}_{\mu,\sigma}(\hat{\mathbf{p}}) \chi^{\xi'}_{\sigma'\sigma} D^1_{\mu,0}(\hat{\mathbf{q}}) D^{j_g,*}_{\Lambda,\lambda'}(\hat{\mathbf{k}}) D^1_{\nu,\lambda}(\hat{\mathbf{k}}) \chi^{\xi}_{\lambda'\lambda} D^{1,*}_{\nu,0}(\hat{\mathbf{q}}) + \eta_Y \eta'_Y(\Lambda \to -\Lambda)], \end{aligned} \tag{A8}$$

where the sum is over μ, ν, λ, λ', σ, σ' and the kernel is given by

$$K(\mathbf{x}, \mathbf{z}, \mathbf{y}) = \int \frac{d\mathbf{k}}{(2\pi)^3} \frac{d\mathbf{p}}{(2\pi)^3} \frac{d\mathbf{q}}{(2\pi)^3} K(k, q, p) e^{i\mathbf{x}\cdot\mathbf{k}} e^{i\mathbf{y}\cdot\mathbf{p}} e^{i\mathbf{z}\cdot\mathbf{q}} \tag{A9}$$

and

$$K(k, q, p) = q^2 \frac{N_C^2}{4} \frac{d(k)d(p)d(q)}{k^2 q^2 p^2} [d(k)f(k) + d(p)f(p) + d(q)f(q)]. \tag{A10}$$

Finally,

$$H_{3f} = \sum \int \frac{d\mathbf{k}}{(2\pi)^3} \frac{d\mathbf{p}}{(2\pi)^3} \frac{d\mathbf{q}}{(2\pi)^3} \frac{\phi^*_{m',j'_g}(p)}{\sqrt{2\omega(p)}} \frac{\phi_{m,j_g}(k)}{\sqrt{2\omega(k)}} \int d\mathbf{x} d\mathbf{y} d\mathbf{z} \Big[K\Big(\mathbf{x} - \frac{\mathbf{R}}{2}, \mathbf{z} + \mathbf{y} - \mathbf{x}, \mathbf{y} - \frac{\mathbf{R}}{2}\Big) + (\mathbf{R} \to -\mathbf{R}) \Big]$$
$$\times e^{i\mathbf{x}\cdot\mathbf{k}} e^{i\mathbf{z}\cdot\mathbf{q}} e^{-i\mathbf{y}\cdot\mathbf{p}} \frac{\sqrt{(2j'_g+1)(2j_g+1)}}{8\pi} [D^{j'_g}_{\Lambda,\sigma'}(\hat{\mathbf{p}}) D^{1,*}_{\mu,\sigma}(\hat{\mathbf{p}}) \chi^{\xi'}_{\sigma'\sigma} D^1_{\mu,0}(\hat{\mathbf{q}}) D^{j_g,*}_{\Lambda,\lambda'}(\hat{\mathbf{k}}) D^1_{\nu,\lambda}(\hat{\mathbf{k}}) \chi^{\xi}_{\lambda'\lambda} D^{1,*}_{\nu,0}(\hat{\mathbf{q}})$$
$$+ \eta_Y \eta'_Y (\Lambda \to -\Lambda)]$$
$$= \sum \int \frac{d\mathbf{k}}{(2\pi)^3} \frac{d\mathbf{p}}{(2\pi)^3} \frac{d\mathbf{q}}{(2\pi)^3} \frac{\phi^*_{m',j'_g}(p)}{\sqrt{2\omega(p)}} \frac{\phi_{m,j_g}(k)}{\sqrt{2\omega(k)}} K(\mathbf{k}+\mathbf{q}, \mathbf{q}, \mathbf{p}+\mathbf{q}) [e^{i(\mathbf{R}/2)\cdot(\mathbf{k}-\mathbf{p})} + (\mathbf{R} \to -\mathbf{R})] \frac{\sqrt{(2j'_g+1)(2j_g+1)}}{8\pi}$$
$$\times [D^{j'_g}_{\Lambda,\sigma'}(\hat{\mathbf{p}}) D^{1,*}_{\mu,\sigma}(\hat{\mathbf{p}}) \chi^{\xi'}_{\sigma'\sigma} D^1_{\mu,0}(\hat{\mathbf{q}}) D^{j_g,*}_{\Lambda,\lambda'}(\hat{\mathbf{k}}) D^1_{\nu,\lambda}(\hat{\mathbf{k}}) \chi^{\xi}_{\lambda'\lambda} D^{1,*}_{\nu,0}(\hat{\mathbf{q}}) + \eta_Y \eta'_Y (\Lambda \to -\Lambda)]. \quad \text{(A11)}$$

In the large-N_C limit, $g\sqrt{N_C} \sim O(1)$, and since $d(k) \propto g$ and $f \sim O(1)$, all of the terms above are $O(1)$ except H_d (which corresponds to a nonplanar diagram, see Fig. 3). The products of the three factors, $d(p_i)/p_i^2$, originate from the three dressed Coulomb lines in Figs. 3(e) and 3(f), and the three factors of Fig. 3(f) come from the three possibilities to insert the ∇^2 operator on these three lines. The derivative coupling between transverse and Coulomb gluons leads to the extra q^2 factor in the numerator in Eq. (A10). In coordinate space this implies that $K(\mathbf{x}, \mathbf{z}, \mathbf{y})$ is short ranged in $\mathbf{z}$. Furthermore in each of the three terms in Eq. (A10) there is only one combination, $d^2(p_i)f(p_i)/p_i^2$, which in momentum space leads to the confining potential V_C. The remaining two are of the form $d(p_i)/p_i^2$ with $d(p) \propto 1/\sqrt{p}$, which for small momenta also leads to a short-ranged interaction decreasing as $1/\sqrt{r}$ for large r. We thus conclude that for the three interaction lines connecting the four vertices in the "-three-body force" of Fig. 3(e) only one is long ranged and all others are short ranged. Along these lines one can approximate $K(\mathbf{x}, \mathbf{z}, \mathbf{y})$ as

$$K(\mathbf{x}, \mathbf{z}, \mathbf{y}) \propto \delta(\mathbf{z}) \Big[\frac{m_g V_C(\mathbf{x})}{(m_g|\mathbf{y}|)^\alpha} + \frac{m_g V_C(\mathbf{y})}{(m_g|\mathbf{x}|)^\alpha} \Big], \quad \text{(A12)}$$

with $0 < \alpha < 1$. Ignoring the gluon spin and all spin-orbit couplings we then obtain

$$H_{3e} \to \int d\mathbf{x} d\mathbf{y} \frac{\phi^*_{m'}(\mathbf{x})}{\sqrt{2m_g}} \frac{\phi_m(\mathbf{y})}{\sqrt{2m_g}} \Big[K\Big(\mathbf{x} - \frac{\mathbf{R}}{2}, \mathbf{y} - \mathbf{x}, \mathbf{y} + \frac{\mathbf{R}}{2}\Big) + (\mathbf{R} \to -\mathbf{R}) \Big]$$
$$\propto \int d\mathbf{x} \phi^*_{m'}(\mathbf{x}) \Big[\frac{V_C(\mathbf{x} - \frac{\mathbf{R}}{2})}{(m_g|\mathbf{x} + \frac{\mathbf{R}}{2}|)^\alpha} + (\mathbf{R} \to -\mathbf{R}) \Big] \phi_m(\mathbf{x}). \quad \text{(A13)}$$

At large separation R with the wave functions peaking at $|\mathbf{x}| \sim 0$, we find that H_e grows less rapidly than two-body interactions. This is in general true for interactions originating from the expansion of $K[A]$ in powers of A which couple multiple gluons. This is the basis for the approximations discussed in Sec. IVA.

The off-diagonal matrix element of the Hamiltonian mixing the $|q\bar{q}\rangle$ and $q\bar{q}g\rangle$ states, shown in Fig. 4, is given by

$$H_4 = i \sum \int \frac{d\mathbf{k}}{(2\pi)^3} \frac{d\mathbf{q}}{(2\pi)^3} \frac{\phi_{m,j_g}(k)}{\sqrt{2\omega(k)}} \int d\mathbf{x} d\mathbf{z} \Big[K_1\Big(\mathbf{x} - \frac{\mathbf{R}}{2}, \mathbf{z} - \mathbf{x} - \frac{\mathbf{R}}{2}\Big) - (\mathbf{R} \to -\mathbf{R}) \Big] e^{i\mathbf{x}\cdot\mathbf{k}} e^{i\mathbf{z}\cdot\mathbf{q}} \frac{\sqrt{2j_g+1}}{4\pi}$$
$$\times D^{j_g,*}_{\Lambda=0,\lambda'}(\hat{\mathbf{k}}) D^1_{\nu,\lambda}(\hat{\mathbf{k}}) \chi^{\xi}_{\lambda'\lambda} D^{1,*}_{\nu,0}(\hat{\mathbf{q}}) = i \sum \int \frac{d\mathbf{k}}{(2\pi)^3} \frac{d\mathbf{q}}{(2\pi)^3} \frac{\phi_{m,j_g}(k)}{\sqrt{2\omega(k)}} K_1(\mathbf{k}+\mathbf{q}, \mathbf{q}) [e^{i(\mathbf{R}/2)\cdot(\mathbf{k}+2\mathbf{q})} - (\mathbf{R} \to -\mathbf{R})]$$
$$\times \frac{\sqrt{2j_g+1}}{4\pi} D^{j_g,*}_{\Lambda=0,\lambda'}(\hat{\mathbf{k}}) D^1_{\nu,\lambda}(\hat{\mathbf{k}}) \chi^{\xi}_{\lambda'\lambda} D^{1,*}_{\nu,0}(\hat{\mathbf{q}}), \quad \text{(A14)}$$

$$K_1(\mathbf{x}, \mathbf{y}) = \int \frac{d\mathbf{p}}{(2\pi)^3} \frac{d\mathbf{q}}{(2\pi)^3} K(p, q) e^{i\mathbf{x}\cdot\mathbf{p}} e^{i\mathbf{y}\cdot\mathbf{q}} \tag{A15}$$

with

$$K_1(p, q) = \frac{N_C\sqrt{C_F}}{2} q \frac{d(p)d(q)}{p^2q^2}[d(p)f(p) + d(q)f(q)]. \tag{A16}$$

As expected in the large N_C limit $K_1 = O(1)$ and just like the three-body kernel described previously, $K_1(\mathbf{x}, \mathbf{y})$ has mixed behavior for large separations. A term, in momentum space, proportional to $d^2 f$ in one of the two momentum variables leads to V_C in the corresponding position space argument. While for the other momentum variable it leads to a less singular behavior for large distances. Approximately, we find

$$K_1\left(\mathbf{x} - \frac{\mathbf{R}}{2}, \mathbf{x} + \frac{\mathbf{R}}{2}\right) \propto \frac{m_g^2 V_C(|\mathbf{x} - \frac{\mathbf{R}}{2}|)}{(m_g|\mathbf{x} + \frac{\mathbf{R}}{2}|)^\beta} + (\mathbf{R} \to -\mathbf{R}) \tag{A17}$$

with $1 < \beta < 2$. In this limit, ignoring spin dependence, one finds

$$H_4 \to i \int d\mathbf{x} K_1\left(\left|\mathbf{x} - \frac{\mathbf{R}}{2}\right|, \left|\mathbf{x} + \frac{\mathbf{R}}{2}\right|\right) \frac{\phi_{m,j_g}(x)}{\sqrt{2m_g}}. \tag{A18}$$

Thus, similar to the case of H_{3e}, we find that at large separations the mixing terms grow less rapidly with R as compared to two-body interactions.

[1] K. J. Juge, J. Kuti, and C. J. Morningstar, Nucl. Phys. B, Proc. Suppl. **63**, 326 (1998).
[2] K. J. Juge, J. Kuti, and C. Morningstar, Phys. Rev. Lett. **90**, 161601 (2003).
[3] T. T. Takahashi and H. Suganuma, Phys. Rev. D **70**, 074506 (2004).
[4] M. Luscher and P. Weisz, J. High Energy Phys. 07 (2004) 014.
[5] J. M. Cornwall, Phys. Rev. D **71**, 056002 (2005).
[6] J. Greensite and C. B. Thorn, J. High Energy Phys. 02 (2002) 014.
[7] G. S. Bali, H. Neff, T. Duessel, T. Lippert, and K. Schilling (SESAM Collaboration), Phys. Rev. D **71**, 114513 (2005).
[8] G. S. Bali, Phys. Rev. D **62**, 114503 (2000).
[9] K. J. Juge, J. Kuti, and C. Morningstar, hep-lat/0401032.
[10] J. Greensite, Prog. Part. Nucl. Phys. **51**, 1 (2003).
[11] K. J. Juge, J. Kuti, and C. J. Morningstar, Phys. Rev. Lett. **82**, 4400 (1999).
[12] K. J. Juge, J. Kuti, and C. J. Morningstar, Nucl. Phys. B, Proc. Suppl. **83**, 304 (2000).
[13] P. Hasenfratz, R. R. Horgan, J. Kuti, and J. M. Richard, Phys. Lett. **95B**, 299 (1980).
[14] K. J. Juge, J. Kuti, and C. J. Morningstar, Nucl. Phys. B, Proc. Suppl. **63**, 543 (1998).
[15] N. Isgur and J. Paton, Phys. Rev. D **31**, 2910 (1985).
[16] D. Horn and J. Mandula, Phys. Rev. D **17**, 898 (1978).
[17] E. S. Swanson and A. P. Szczepaniak, Phys. Rev. D **59**, 014035 (1999).
[18] K. J. Juge, J. Kuti, and C. Morningstar, hep-lat/0312019.
[19] C. B. Thorn, Phys. Rev. D **20**, 1435 (1979).
[20] A. P. Szczepaniak and E. S. Swanson, Phys. Rev. D **55**, 3987 (1997).
[21] J. Greensite and S. Olejnik, Phys. Rev. D **67**, 094503 (2003).
[22] J. Greensite, S. Olejnik, and D. Zwanziger, Phys. Rev. D **69**, 074506 (2004).
[23] D. Zwanziger, Phys. Rev. Lett. **90**, 102001 (2003).
[24] N. H. Christ and T. D. Lee, Phys. Rev. D **22**, 939 (1980).
[25] P. van Baal, hep-th/9711070.
[26] H. Reinhardt and C. Feuchter, Phys. Rev. D **71**, 105002 (2005).
[27] C. Feuchter and H. Reinhardt, Phys. Rev. D **70**, 105021 (2004).
[28] A. P. Szczepaniak, Phys. Rev. D **69**, 074031 (2004).
[29] A. P. Szczepaniak and E. S. Swanson, Phys. Rev. D **65**, 025012 (2002).
[30] K. Langfeld and L. Moyaerts, Phys. Rev. D **70**, 074507 (2004).
[31] S. L. Adler and A. C. Davis, Nucl. Phys. **B244**, 469 (1984).
[32] A. Szczepaniak, E. S. Swanson, C. R. Ji, and S. R. Cotanch, Phys. Rev. Lett. **76**, 2011 (1996).
[33] N. Ligterink and E. S. Swanson, Phys. Rev. C **69**, 025204 (2004).
[34] A. P. Szczepaniak and E. S. Swanson, Phys. Lett. B **577**, 61 (2003).
[35] C. J. Morningstar (private communication).